JANUARY 20, 2012 VOLUME 287 NUMBER 4

ASBMB AMERICAN SOCIETY FOR BIOCHEMISTRY AND MOLECULAR BIOLOGY

Critical Role for Heat Shock Protein 20 (HSP20) in Migration of Malarial Sporozoites*^{*}

Received for publication, September 9, 2011, and in revised form, November 7, 2011 Published, JBC Papers in Press, December 2, 2011, DOI 10.1074/jbc.M111.302109

Georgina N. Montagna[‡], Carlos A. Buscaglia[§], Sylvia Münter[¶], Christian Goosmann[‡], Friedrich Frischknecht[¶], Volker Brinkmann[‡], and Kai Matuschewski^{‡1}

From the [†]Max Planck Institute for Infection Biology, 10117 Berlin, Germany, [§]Instituto de Investigaciones Biotecnológicas (IIB-INTECH), Universidad Nacional de San Martín, 1650 San Martín, Buenos Aires, Argentina, and [¶]Department of Infectious Diseases, Heidelberg University School of Medicine, 69120 Heidelberg, Germany

Background: Small heat shock proteins have been associated with microfilament regulation.

Results: Ablation of HSP20 impairs the speed, directionality, and adhesion of Plasmodium sporozoites.

Conclusion: HSP20 is a key factor for locomotion and infection of the malaria parasite.

Significance: This study is the first genetic evidence for a role of a small heat shock protein in cellular motility.

Plasmodium sporozoites, single cell eukaryotic pathogens, use their own actin/myosin-based motor machinery for life cycle progression, which includes forward locomotion, penetration of cellular barriers, and invasion of target cells. To display fast gliding motility, the parasite uses a high turnover of actin polymerization and adhesion sites. Paradoxically, only a few classic actin regulatory proteins appear to be encoded in the Plasmodium genome. Small heat shock proteins have been associated with cytoskeleton modulation in various biological processes. In this study, we identify HSP20 as a novel player in Plasmodium motility and provide molecular genetics evidence for a critical role of a small heat shock protein in cell traction and motility. We demonstrate that HSP20 ablation profoundly affects sporozoite-substrate adhesion, which translates into aberrant speed and directionality in vitro. Loss of HSP20 function impairs migration in the host, an important sporozoite trait required to find a blood vessel and reach the liver after being deposited in the skin by the mosquito. Our study also shows that fast locomotion of sporozoites is crucial during natural malaria transmission.

Substrate-dependent motility in eukaryotic cells depends on regulated turnover of filamentous actin (F-actin) (1, 2). A plethora of actin-binding proteins regulate the highly dynamic equilibrium between globular (*G*-) and F-actin by actin sequestra-

tion, modulation of the actin ATPase activity, or catalyzing nucleotide exchange (1). One inhibitor of actin polymerization was purified and identified as a small heat shock protein $(sHSP)^2$ (3, 4). The family of sHSPs encodes ubiquitous proteins that function in various cellular processes, including maintenance of cellular homeostasis and a balanced redox environment (5, 6). Their unifying features include a carboxyl-terminal \sim 10-kDa α -crystallin domain, the propensity to form large oligomeric complexes, and chaperone activity (7, 8). In addition to their roles as molecular chaperones, sHSPs are recognized for their participation in protein trafficking, signal transduction, and cytoskeleton dynamics. The latter function is supported by biochemical and limited genetic data (9-12). To explain the roles of sHSPs in actin dynamics, alternative modes of action, including direct competition with myosin binding to F-actin (13), alteration of actin attachment sites at membranedense plaques and cytoplasmic dense bodies (14), and sequestration of the 14-3-3 protein, resulting in liberation of cofilin (15, 16), have been proposed. However, whether chaperones play an important role in microfilament-dependent processes in vivo still remains an open question.

Apicomplexan parasites are single cell eukaryotic pathogens with an obligate intracellular life style. To progress in their complex life cycles, these parasite form motile extracellular stages, which utilize their own actin/myosin motor for fast, substrate-dependent locomotion (17, 18). Molecular and chemical genetics data in Toxoplasma gondii and Plasmodium berghei revealed a central role for an unconventional class XIV myosin A in complex with its light chain in the gliding process (19-22). Class XIV myosin A moves along short and dynamic actin filaments (18, 23-26), which in turn interact with the cytoplasmic tail of transmembrane proteins of the thrombospondin-related anonymous protein (TRAP) family (27, 28) likely via aldolase tetramers (29-31). Because the extracellular adhesive domains of TRAP family proteins are tightly anchored to the substrate, backward translocation of actin filaments translates into forward movement of the parasite.

² The abbreviations used are: sHSP, small heat shock protein; RICM, reflection interference contrast microscopy; TRAP, thrombospondin-related anonymous protein; CSP, circumsporozoite protein.



^{*} This work was supported by the European Commission (European Virtual Institute for Malaria Research Grants 2 and 34 to F. F. and K. M.); the Max Planck Society, the Joachim Siebeneicher Foundation, and the Chica and Heinz Schaller Foundation (to K. M.); the German Ministry of Education and Research (Bundesministerium für Bildung und Forschung, BioFuture program) and the Frontier Program of the University of Heidelberg (to F. F.); the von Humboldt Foundation (to G. N. M.); and the Agencia Nacional de Promoción Científica y Tecnológica (Argentina) and the United Nations Children's Fund/United Nations Development Program/World Bank/World Health Organization Special Program for Research and Training in Tropical Diseases (to C. A. B.).

This article contains supplemental Experimental Procedures, Figs. 1–5, and Movies 1–6.

¹To whom correspondence should be addressed: Parasitology Unit, Max Planck Inst. for Infection Biology, 10117 Berlin, Germany. Tel.: 49-30-28460535; Fax: 49-30-28460225; E-mail: matuschewski@mpiib-berlin.mpg. de.

Low doses of actin filament-stabilizing drugs, such as jasplakinolide, increase parasite velocity, thus indicating that filament formation is a rate-limiting step in *Plasmodium* motility (32–34). Indeed, apicomplexan actin exhibits unusual dynamic properties: in vitro studies have shown that it can be rapidly polymerized into microfilaments at a 3-4-fold lower critical concentration than mammalian muscle actin (26). However, in vivo actin apparently is maintained largely in a globular state (33). Stabilization of G-actin is mediated by at least three abundant G-actin-binding proteins, i.e. profilin (35, 36), actin-depolymerizing factor 1 (37, 38), and the small cyclase-associated protein (39). These findings indicate that our understanding of the molecular basis of the apicomplexan motor machinery is still incomplete and possibly lacks additional, yet unidentified proteins that orchestrate actin dynamics and parasite motility. Database mining returned a very limited repertoire of classical actin-binding proteins in apicomplexans as compared with other eukaryotes (40, 41).

Interestingly, one sHSP member, termed HSP20, from T. gondii was recently shown to co-localize with the motor complex at the outer surface of the inner membrane complex (42). This unique subcellular localization indicates that TgHSP20 may play a role in apicomplexan motility. In this study, we used experimental genetics to address the roles of HSP20 in life cycle progression of the malarial parasite. We show that HSP20 is critical for fast sporozoite locomotion in vitro and for efficient natural malaria transmission in vivo.

EXPERIMENTAL PROCEDURES

Experimental Animals—All animal work was conducted in accordance with the German Animal Protection Law (version May 18, 2006), which implements the directive 86/609/EEC from the European Union and the European Convention for the protection of vertebrate animals used for experimental and other scientific purposes. The protocol was approved by the ethics committee of the Max Planck Institute for Infection Biology and the Berlin state authorities (Landesamt für Gesundheit und Soziales (LAGeSo) registration number G0469/09).

Plasmodium Life Cycle—P. berghei parasites (ANKA strain), which constitutively express GFP under the control of the EF1 α promoter (43), and the corresponding parental, non-fluorescent parasites were used. Parasite life cycle progression and phenotyping was done as described in the supplemental Experimental Procedures. Monoclonal antibodies against P. berghei circumsporozoite protein (CSP) (44) and heat shock protein 70 (45) were used to label sporozoites and exoerythrocytic forms, respectively.

Transmigration and Invasion Assays—For analysis of sporozoite cell traversal, HuH7 or human foreskin fibroblast cells were incubated for 3 h with 5×10^4 sporozoites in the presence of 0.5 mg/ml fluorescein-conjugated dextran (Molecular Probes). Cells were then trypsinized, washed to remove extracellular sporozoites and dextran, and either analyzed by FACS to determinate the percentage of dextran-positive cells or plated in eight-chamber plastic Lab-Tek slides and further cultured for at least 6 h before analysis by fluorescence microscopy using the PbHSP70 antibody (45). To determine sporozoite invasion, 5×10^4 sporozoites were incubated with HuH7 cells for 1 h and fixed with 4% paraformaldehyde. We used two-color labeling using the P. berghei CSP antibody (44) to distinguish intra- (double labeled) from extracellular (single labeled) sporozoites.

Recombinant Protein Expression and Antiserum Production— The full-length PbHSP20 ORF was expressed in a GST expression plasmid as described previously (30). For the production of specific antiserum, 50 μg of GST-PbHSP20 suspended in PBS were emulsified in complete Freund's adjuvant (Sigma-Aldrich) and injected into male mice (C3H/HeN) by the intraperitoneal route. Two boosters of 10 µg each in incomplete Freund's adjuvant (Sigma-Aldrich) were given at days 15 and 25 postinjection. Two weeks after the second boost, blood was collected, and serum was isolated. Specificity of the anti-Pb-HSP20 antiserum was evaluated by reactivity toward the His₆tagged version of the protein.

Microscopy Techniques-Salivary gland sporozoites were deposited onto bovine serum albumin-coated microscopic dishes (Ibidi GmbH, Martinsried, Germany). Areas with sufficient density of attached sporozoites were identified by wide field light microscopy and marked under the dishes. Pre-embedding labeling, embedding, and sectioning for electron microscopy were performed as described (46). For cryoimmunoelectron microscopy, infected salivary glands were fixed with 2% paraformaldehyde and 0.05% glutaraldehyde and stained en block with DRAQ5TM (Biostatus Ltd., Shepshed, UK) DNA dye for later identification of the tissue. Samples were then cryopreserved and sectioned as described previously (46). Transmission EM samples were analyzed in a LEO 906 (Zeiss, Oberkochen, Germany) transmission electron microscope equipped with a Morada (Olympus Soft Imaging Solutions, Munster, Germany) side-mounted digital camera. For scanning electron microscopy of gliding sporozoites, salivary gland sporozoites were deposited onto bovine serum albumin-coated glass slides and incubated at 37 °C. After fixation with 2% paraformaldehyde, samples were labeled as described (46). As secondary antibody, we used 40-nm gold-conjugated anti-mouse Ig antibody (British Biocell, Cardiff, UK). Imaging was performed using both in-lens and back-scatter signals in a LEO 1550 (Zeiss) scanning electron microscope at 20-kV acceleration voltage. For reflection interference contrast microscopy (RICM), the RICM setup was mounted on an inverted Axiovert 200 Zeiss microscope with an Antiflex Plan-Neofluar 63× objective (numerical aperture, 1.25) using the 546.1-nm line of a mercury lamp. Images of sporozoites in glass bottom dishes were recorded with a charge-coupled device camera (AxioCam, Zeiss) using AxioVision software (Zeiss). Gliding motility of in vitro cultured ookinetes was recorded as described (47). Time lapse videos (one frame every 2 s for 5 min) were taken with a Zeiss Axiovert 200M microscope. The speed of individual ookinetes was calculated by manual tracking using the manual tracking plug-in of ImageJ software. The Mann-Whitney nonparametric test was used to calculate the statistical significance of differences (**, p < 0.05). Live imaging of intradermal sporozoite migration was performed at 37 °C as described (48) using a Leica SP5 confocal microscope. Images were collected with LASAF software analyzed using ImageJ Volocity (Improvision). Pixel sizes were preserved during images processing. The speed

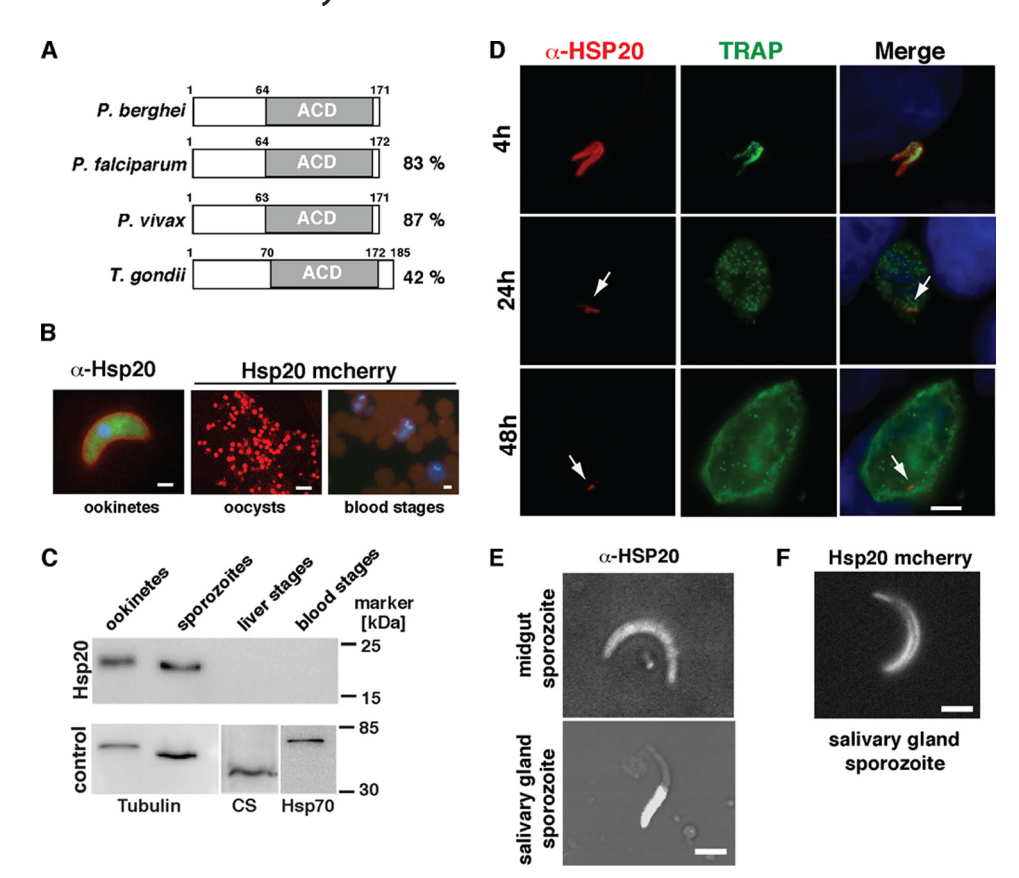


FIGURE 1. **Expression of HSP20 during Plasmodium life cycle.** *A*, protein structure of apicomplexan HSP20 members. HSP20 from *P. berghei* (gi:68076145; PBANKA_071430), *Plasmodium falciparum* (gi:124512452; MAL8P1.78), *Plasmodium vivax* (gi:148803880; PVX_089585), and *T. gondii* (gi:211965817; TGME49_032940) are shown schematically. The percentage of amino acid sequence identity compared with *PbHSP20* is indicated to the *right*. The *gray box* represents the conserved α -crystallin domain (*ACD*). *B*, HSP20 is primarily expressed in insect stages of the malaria parasite. Life cycle stages of transgenic parasites were analyzed directly by epifluorescence microscopy (*red*) or in the case of ookinetes (*left*) by indirect immunofluorescence microscopy using the *PbHSP20* antiserum. Nuclei were stained with Hoechst 33342 (*blue*). *Scale bars*, ookinetes, 2 μ m; oocysts, 40 μ m; blood stages, 5 μ m. *C*, HSP20 protein is expressed predominantly in ookinetes and sporozoites. Shown is a Western blot analysis of ookinete and sporozoite extracts, infected hepatoma cells isolated 24 h after infection with *P. berghei* sporozoites, and mixed blood stages. The *PbHSP20* antiserum specifically recognizes a protein that closely resembles the predicted size (18 kDa). Anti-tubulin antibody was used as a loading control for ookinetes and sporozoites. Anti-CS and anti-HSP70 antibodies were used as liver and blood stage loading controls, respectively. *D*, HSP20 is progressively lost during liver stage maturation. Shown are early (4 h) and late hepatic stages (24 and 48 h). Indirect immunofluorescence microscopy of liver stages stained with anti-HSP20 (*red*) and anti-TRAP antibody (*green*) is shown. *White arrows* indicate HSP20 staining. *Scale bars*, 5 μ m. *E*, HSP20 in midgut and salivary gland sporozoites. Sporozoites were allowed to glide on serum albumin-coated glass slides before fixation and permeabilization followed by staining with the anti-HSP20 antiserum. *Scale bar*, 2 μ m. *F*, still image of a gl

of individual sporozoites was calculated by manual tracking at the apical end using the manual tracking plug-in of ImageJ and compared with the automatic tracking using the "Measurement" package of Volocity. Based on these data, displacement, track length, and meandering index were calculated using Volocity. The Mann-Whitney non-parametric test was used to calculate the statistical significance of differences (**, p < 0.05).

RESULTS

Small Heat Shock Protein HSP20 in Malaria Parasites—To look for candidate orthologs of HSP20 in Plasmodium, we performed homology searches in the malaria genome database (49) using the TgHSP20 sequence (gi: 78368731) as query. As expected, we identified a putative HSP20 that is highly conserved across the *Plasmodium* genus (Fig. 1*A* and supplemental Fig. 1). Importantly, all *Plasmodium* HSP20 proteins contain a central α -crystallin domain (Pfam: PF00011), a unifying feature of eukaryotic sHSPs (8, 50).

HSP20 Is Predominantly Expressed in Mosquito Stages—We initiated our analysis by profiling PbHSP20 (gi: 68076145;

PBANKA_071430) expression in different P. berghei life cycle stages. To that end, we generated a parasite line expressing an additional copy of HSP20 fused to the red fluorescent protein mCherry (51) under the control of the endogenous promoter (Fig. 1B and supplemental Fig. 2). In addition, we generated a polyclonal antibody against purified recombinant PbHSP20. We monitored *Pb*HSP20 expression during *Plasmodium* life cycle progression using confocal microscopy and Western blot analysis (Fig. 1, B-D). PbHSP20 was abundantly expressed in insect stages, namely in ookinetes, oocysts, and sporozoites. In contrast, fluorescent signals in the stages within the mammalian host, e.g. asexual erythrocytic stages, were barely detectable. This drastic reduction in PbHSP20 expression during the transition from mosquito to the vertebrate host became even more evident when we monitored liver stages, the first parasite expansion phase preceding pathogenic blood infection (Fig. 1D and supplemental Fig. 2C). We analyzed the expression of this protein in infected hepatoma cells with a polyclonal antibody generated against



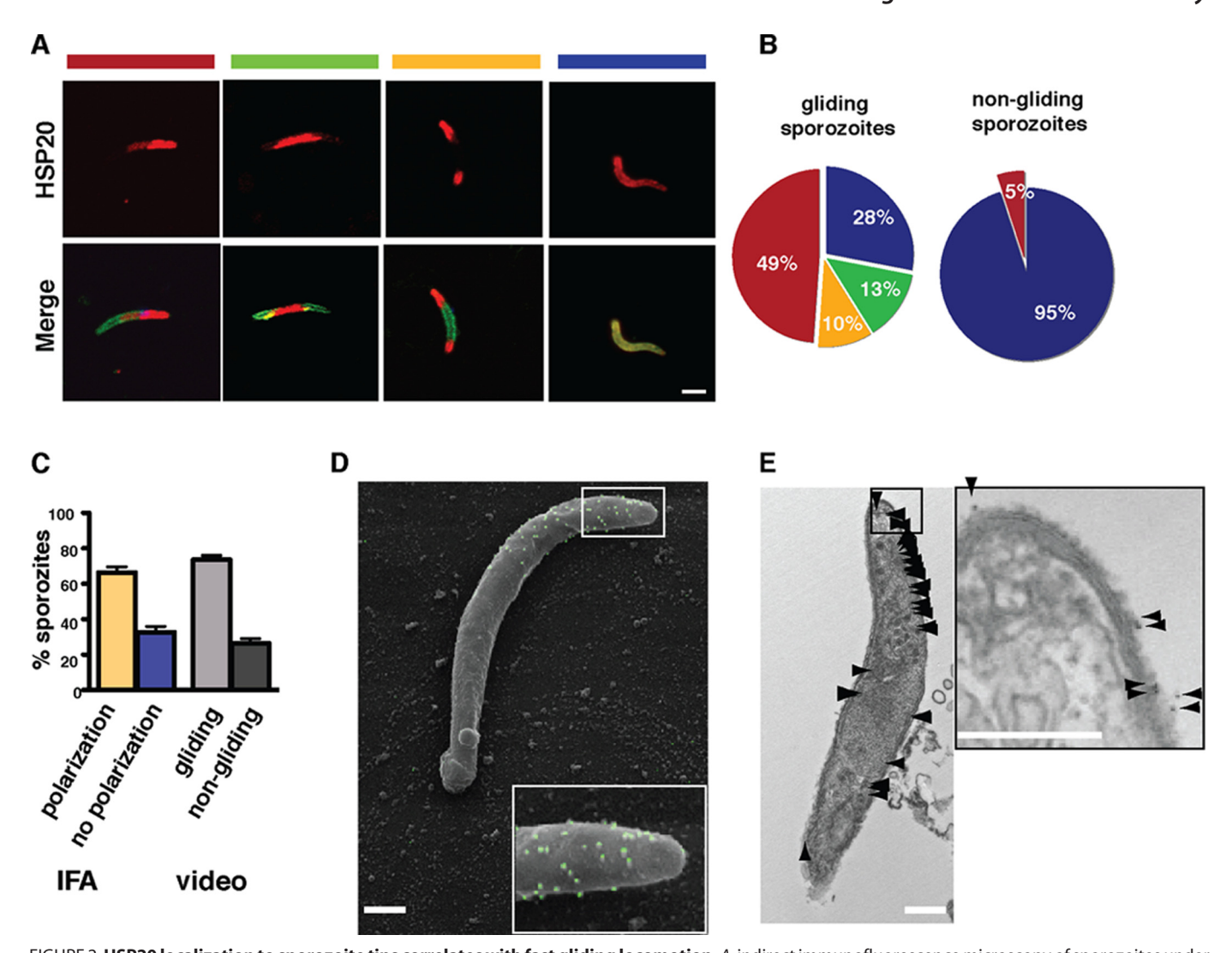


FIGURE 2. HSP20 localization to sporozoite tips correlates with fast gliding locomotion. A, indirect immunofluorescence microscopy of sporozoites under gliding and non-gliding conditions. Fixed and saponin-permeabilized sporozoites were labeled with anti-HSP20 (red) and anti-actin (green) antisera. Shown are representative images of the four distinct HSP20 localization patterns observed in sporozoites: parasite tip (red bar), central region (green bar), bipolar (orange bar), and uniform distribution (blue bar). Scale bar, 2 μ m. B, quantification of HSP20 localization patterns under gliding (n = 174) and non-gliding (n = 136) conditions. C, correlation between proportions of sporozoites displaying polarized HSP20 localization and gliding locomotion. Localization of HSP20 was done by immunofluorescence assay (IFA), and locomotion was observed by direct video microscopy. D, scanning immunoelectron microscopy of a salivary gland sporozoite. Sporozoites were allowed to glide before fixation with paraformaldehyde and saponin permeabilization. Sporozoites were incubated with the PbHSP20 antiserum followed by 40-nm gold labeling (green dots). Scale bars, 1 µm. Note the HSP20-negative trail and HSP20 labeling at the tip of the sporozoite. The inset contains a higher magnification of the apical sporozoite tip. E, immunoelectron micrograph of a gliding sporozoite. Sporozoites were fixed after gliding, permeabilized with saponin, and incubated with anti-HSP20 followed by labeling with 6-nm gold particles. Sporozoite longitudinal sections were analyzed by transmission microscopy. Black arrows denote the position of gold particles as exemplified in the higher magnification of the sporozoite tip in the inset. Scale bars, 0.5 μm.

the purified recombinant PbHSP20 protein. At 4 h after hepatocyte invasion, the HSP20 signal, likely derived from the infecting sporozoite, was still clearly detectable. This signal was progressively lost from later stage parasites and was no longer detectable in mature liver stages (48 h). Remarkably, at early time points, HSP20 appeared to be restricted to a small area at the parasite periphery. This labeling pattern and its subsequent loss are reminiscent of the inner membrane complex, which is dismantled during sporozoite metamorphosis in the liver (20, 52, 53).

HSP20 Is Redistributed to Apical Tip in Motile Sporozoites— Using the PbHSP20 antibody, we detected a uniform and peripheral distribution of HSP20 in midgut-associated sporozoites (Fig. 1E). Unexpectedly, a substantial proportion (70%) of

salivary gland-associated sporozoites displayed a polarized distribution of HSP20. Although morphologically similar, midgutand salivary gland-associated sporozoites profoundly differ in their capacity to glide on solid substrates, which likely contributes to their differential infectivity to the mammalian host (54,

To evaluate whether the contrasting HSP20 distribution in distinct sporozoite populations correlated with their differential gliding capacity, we analyzed PbHSP20 staining patterns in salivary gland sporozoites incubated under gliding and nongliding conditions (Fig. 2). PbHSP20 displayed a non-homogeneous distribution in the majority (70%) of sporozoites incubated under gliding conditions (Fig. 2A). Under this category, we include parasites showing HSP20 accumulation at either

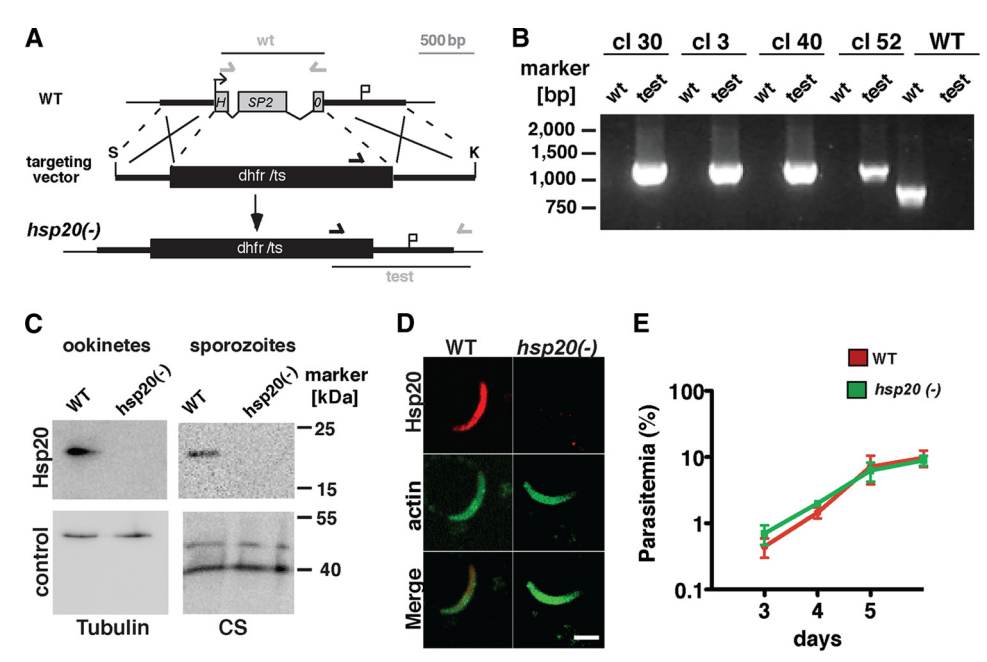


FIGURE 3. **Targeted gene deletion of** *P. berghei HSP20* **does not affect blood infection.** *A*, replacement strategy to generate hsp20(-) parasites. The *PbHSP20* genomic locus was targeted with a replacement plasmid containing 5'- and 3'-regions flanking the *HSP20* ORF (*black bars*) and the *Tgdhfr/ts* positive selectable marker. Replacement and wild type-specific test primer combinations and expected fragments are indicated. *B*, genotyping of hsp20(-) parasites. Confirmation of the predicted gene replacement was achieved by PCR analysis using a primer combination (*test*) that only amplifies a signal from the recombinant locus. A wild type-specific primer combination (*wt*) confirms the absence of residual wild type parasites in the clonal (*cl*) hsp20(-) populations. *C*, HSP20 protein is absent in hsp20(-) parasites. Shown is a Western blot analysis of WT and hsp20(-) ookinete and sporozoite extracts. The anti-*PbHSP20* antiserum specifically recognizes a protein that closely resembles the predicted size (18 kDa). Anti-tubulin and anti-circumsporozoite protein antibodies are used as loading controls. *D*, immunofluorescence microscopy confirms the successful deletion of *HSP20*. The *PbHSP20* antiserum shows the typical polarized signal in WT sporozoites, whereas no signal is detectable in hsp20(-) parasites. *Scale bar*, 2 μ m. *E*, asexual blood stage development is unaffected in hsp20(-) parasites. Mice were infected intravenously with 1,000 infected erythrocytes. Parasitemia of recipient mice (n = 5) was monitored daily by examination of Giemsa-stained blood smears. Shown are mean values (\pm S.D.) (*error bars* \pm S.D.). *K*, *kpnI*; *S*, *Sac* II; *HSP20*, heat shock protein 20.

one or both parasite tips and those that display a distinct HSP20 signal in the center of the parasite. Interestingly, the percentage of parasite displaying polarized HSP20 distribution was similar to the proportion of sporozoites performing gliding locomotion (Fig. 2, *B* and *C*). The remaining 30% of the population showed an overall weaker HSP20 signal and a rather uniform distribution, which is highly reminiscent of what was observed in midgut sporozoites (Fig. 1*E*). This population likely represents sporozoites that remained immotile during the assay (Fig. 2*C*). To corroborate our findings, we performed live cell imaging of transgenic *HSP20-mCherry* sporozoites (Fig. 1*F* and supplemental Movie 1). In gliding sporozoites, tagged *Pb*HSP20 localized to the plasma membrane of gliding sporozoites and accumulated at the ventral side of the anterior tip and at the posterior half.

We next carried out immunoscanning electron microscopy on sporozoites that were permitted to glide on glass coverslips before fixation and permeabilization (Fig. 2D and supplemental Fig. 3). In some cases, we were able to visualize sporozoite trails, all of which lacked an HSP20 signal (Fig. 2D). Moreover, peripheral HSP20, which was likely accessible to antibodies following saponin permeabilization, preferentially accumulated at the tips of curved sporozoites reflecting previous circular locomotion. Under non-gliding conditions, only a few HSP20-specific signals, which were evenly scattered along the entire parasite surface, were detectable (supplemental Fig. 3C).

Next, we performed immunoelectron microscopy with the *Pb*HSP20 antibody on sections of gliding sporozoites that were

permeabilized with saponin (Fig. 2*E*). Accumulation of the gold particles at the sporozoite tips lends further support to the notion that polar distribution of HSP20 correlates with active locomotion. Together, our data suggest that HSP20 is recruited to the cortical side of the pellicle in gliding sporozoites and that this polarization of HSP20 is a molecular signature of mature, motile, and infectious sporozoites.

HSP20 Is Dispensable for Plasmodium Blood and Insect Stages—To study the role(s) of HSP20 in Plasmodium, we performed an experimental genetics approach. We targeted the PbHSP20 gene with a replacement vector, which contains the PbHSP20 5'- and 3'-flanking regions and a positive selection marker cassette (Fig. 3A). Upon a double crossover event, this vector was predicted to delete the entire PbHSP20 locus. After transfection in asexual blood stage and continuous selection with the antifolate pyrimethamine, we obtained a parental population that was further used for parasite cloning. Genotyping assays of four parasite lines confirmed the correct gene replacement event (Fig. 3B). Western blotting and immunofluorescence assays using PbHSP20 antiserum further confirmed the absence of HSP20 in the hsp20(-) parasites (Fig. 3, C and D). Successful generation of HSP20-deficient parasites already indicates that this gene is dispensable during the pathogenic blood stage cycle in vivo in good agreement with our protein expression data (Fig. 1). To support this notion, we monitored parasite replication in mice and could not detect any significant differences between wild type (WT) and hsp20(-) parasites (Fig. 3E).



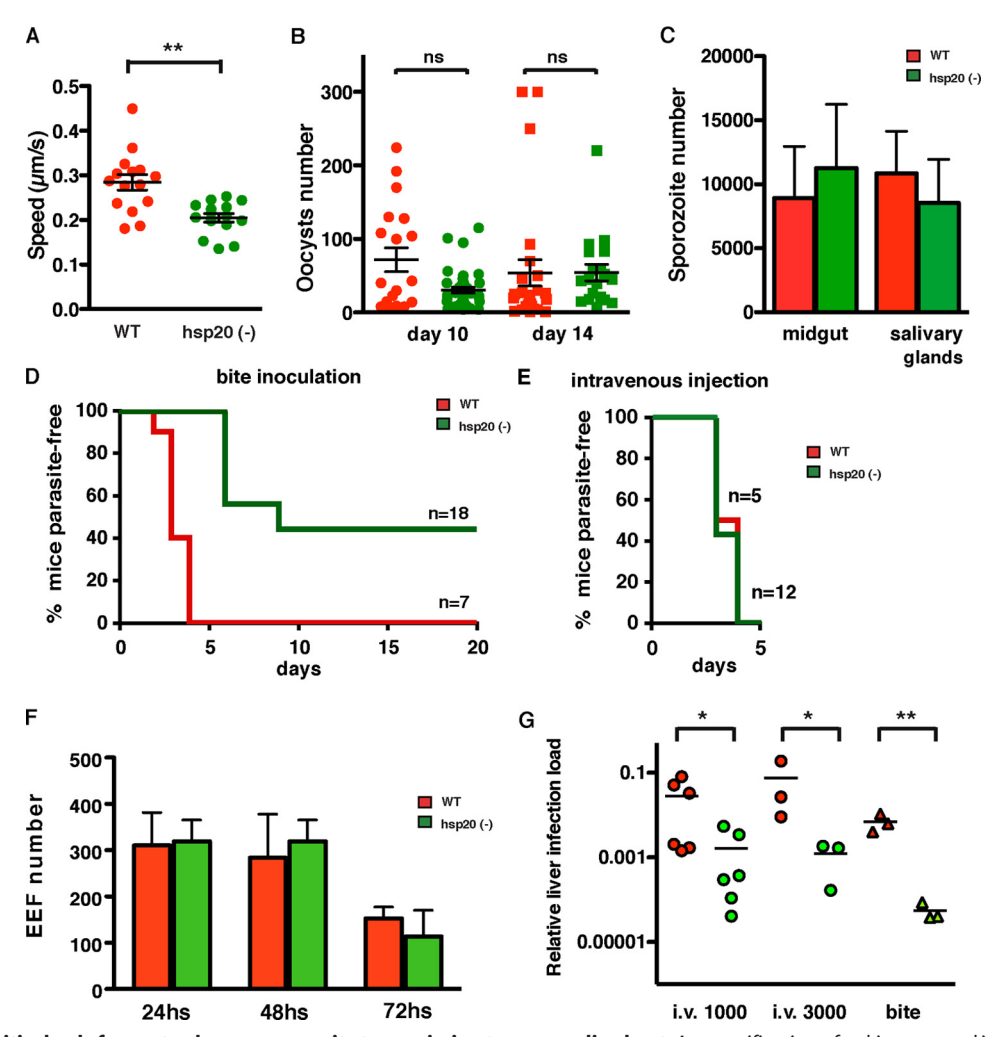


FIGURE 4. **HSP20** is critical only for vector-borne sporozoite transmission to mammalian host. A, quantification of ookinete speed in WT (red) and hsp20(-)(green) parasites. Individual ookinetes were tracked between 1 and 5 min (WT, n = 15; hsp20(-), n = 15). Shown are mean values (\pm S.D.). **, p < 0.05(Mann-Whitney test). B, quantification of mean oocyst numbers (±S.D.) in WT- (red) and hsp20(-) (green)-infected Anopheles stephensi mosquitoes at days 10 and 14 after infection. C, quantification of mean sporozoite numbers (±S.D.) in midgut-associated oocysts (day 14 after infection) and salivary glands (day 17 after infection). D, natural transmission experiments by exposure of mice to three to five WT- and hsp20(-)-infected A. stephensi mosquitoes. Infection was monitored daily by examination of Giemsa-stained blood smears (n, mice per group). E, bypass of natural sporozoite transmission by intravenous injection of sporozoites. Mice were inoculated intravenously with 1,000 sporozoites. F, cultured hepatoma cells were infected with WT and hsp20(-) sporozoites and $cultured for 24, 48, and 72 h before staining with an anti-HSP70 antibody. The results represent mean values (\pm S.D.) of three experiments. \textit{EEF, exoerythrocytic}$ form. G, quantification of parasite loads by real time PCR in infected livers at 42 h after inoculation of WT (red circles) or hsp20(-) (green circles) sporozoites intravenously (i.v.) (left) or by the bite of infected Anopheles mosquitoes. C57bl/6 mice were used, and relative expression levels of the Pb18S gene were normalized to the mouse GAPDH gene. *, p < 0.05; **, p < 0.01 (two-tailed Student's t test); ns, non-significant. Error bars \pm S.D.

We next extended our in vivo analysis to host switch and subsequent mosquito stages (Fig. 4). We first tested whether HSP20 might play a role in ookinete motility. Indeed, the speed of gliding ookinetes obtained from in vitro cultures was moderately, albeit significantly, reduced (Fig. 4A). When we quantified oocyst development, sporozoite formation, and sporozoite accumulation in salivary glands, the target organ in the Anopheles vector, we noticed no significant differences between WT and hsp20(-) parasites (Fig. 4, B and C). These results indicate an auxiliary role of HSP20 in ookinete motility and rule out a major role for HSP20 in the final steps of sporogony in the vector, including efficient colonization of the salivary glands.

hsp20(-) Parasites Are Defective in Natural Malaria *Transmission*—Because hsp20(-) sporozoites developed indistinguishably from WT sporozoites inside the invertebrate host, we were able to study the HSP20 loss-of-function phenotype

during mosquito-to-mouse transmission. When hsp20(-)-infected Anopheles mosquitoes were allowed to blood feed on malaria-naive mice, a strong defect in the infectivity was observed (Fig. 4D). Half of the animals remained entirely malaria-free up to 20 days after challenge, whereas the other half were diagnosed with blood stage infections only after a substantial delay of about 3 days. Because of the exponential (~10-fold) increase of the asexual parasites every 24 h, this difference reflects a dramatic reduction and/or delay in merozoites emerging after liver stage development.

We next bypassed the intradermal phase and injected sporozoites intravenously (Fig. 4E). Intriguingly, hsp20(-) and WT sporozoites showed no differences in infectivity; all animals were blood stage-positive by 3-4 days after sporozoite injection. To support our finding that intrahepatic development is normal, we added WT and hsp20(-) sporozoites to cultured hepatoma cells and quantified exoerythrocytic forms at daily



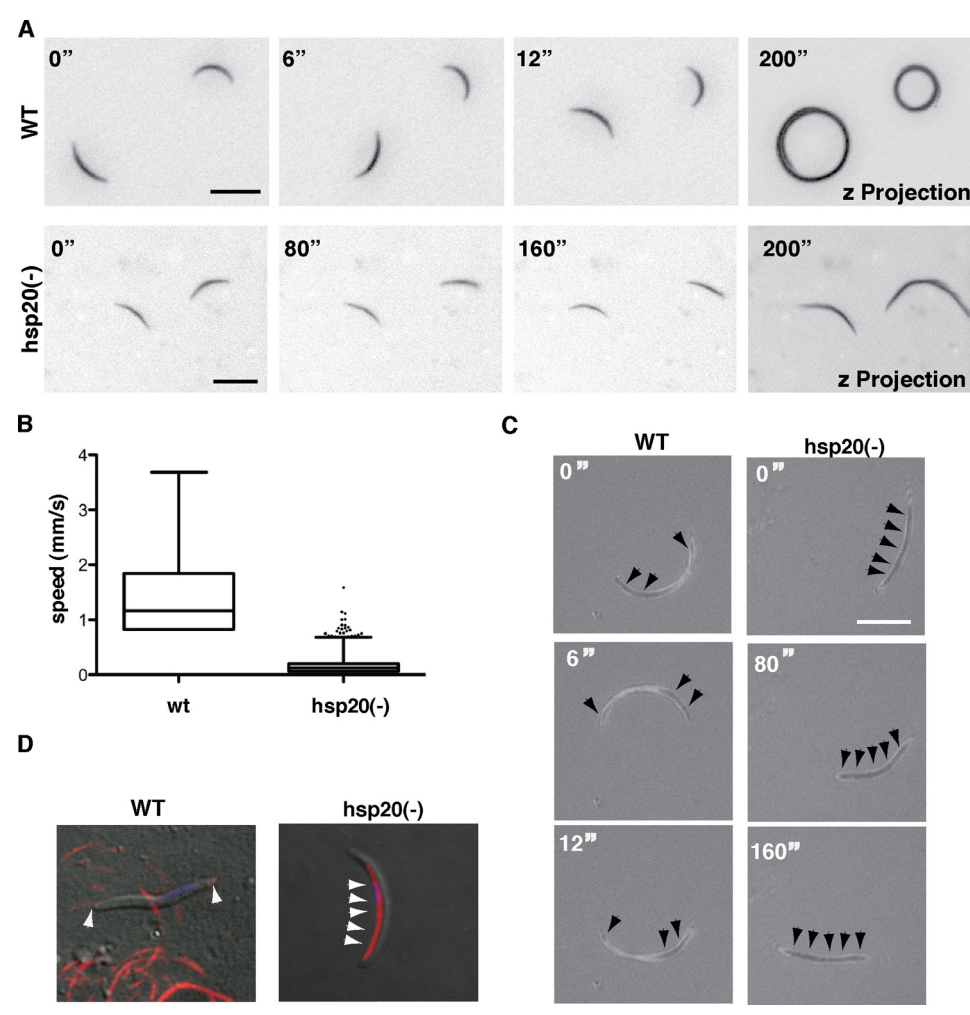


FIGURE 5. **Aberrant gliding locomotion of** hsp20(-) **sporozoites** in **vitro.** A, time series of WT and hsp20(-) parasites with z-projections of the entire time series. Note that WT sporozoites show circular trajectories, whereas hsp20(-) sporozoites show extended trajectories. Scale bars, 10 μ m. B, reduced speed in hsp20(-) sporozoites. The average speed of WT (white) and hsp20(-) (black) sporozoites was quantified from 20 representative sporozoites each. Shown are mean values (\pm S.D.; black dots are outliers). C, RICM images of two representative sporozoites. Left panels show stick-slip motion of WT parasites, and right panels show that hsp20(-) parasites have only one elongated, non-dynamic, attachment site. Arrows indicate the adhesion sites. Scale bars, 5 μ m. D, distribution of the sporozoite adhesin TRAP in gliding WT and hsp20(-) sporozoites. Shown are immunofluorescence images of gliding sporozoites stained with an anti-PbTRAP antiserum (56). TRAP localization on the sporozoite surface is indicated by white arrowheads. Note that TRAP distribution in hsp20(-) sporozoites reflects the elongated adhesion sites detected by RICM (C). Error bars \pm S.D.

intervals (Fig. 4F). No differences were observed between the two parasite lines, demonstrating that hsp20(-) sporozoites retain their full capacity to invade and develop within their final target cells.

To independently quantify the differences in *in vivo* infectivity observed by the two infection routes, we performed quantitative RT-PCR of livers from animals infected either by intravenous injection of sporozoites or by mosquito bite (Fig. 4*G*). This analysis revealed modest and robust reductions of the parasite load, respectively. This finding indicates a strong defect to colonize the liver when sporozoites were transmitted by the natural route. We therefore conclude that *HSP20* plays a critical role for the parasite life cycle only during natural transmission by mosquitoes.

hsp20(-) Parasites Display Aberrant Sporozoite Motility and Substrate Adhesion in Vitro—When we monitored sporozoite locomotion in vitro by video microscopy, we noticed a striking reduction in gliding speed of hsp20(-) sporozoites as compared with WT sporozoites (Fig. 5). Surprisingly, WT sporozo-

ites showed typical circular trajectories, whereas hsp20(-)sporozoites followed extended trajectories (Fig. 5A). Because gliding speed is strongly determined by adhesion to the substrate (34), we speculated that the specific motility defect seen in hsp20(-) sporozoites could be related to altered adhesion to the glass surface as a surrogate substrate. To test this hypothesis, we performed RICM studies of both WT and hsp20(-) sporozoites (Fig. 5C and supplemental Movies 2 and 3). Importantly, hsp20(-) sporozoites mainly established a single large adhesion site spanning almost the entire parasite length. In WT parasites, several distinct adhesion sites were found (Fig. 5C) as described recently (34). Additionally, although WT sporozoites continuously form and disrupt their substrate contacts, hsp20(−) sporozoites showed a highly reduced rate of adhesion turnover. To corroborate our findings, we labeled the vital sporozoite adhesin TRAP (56) and detected TRAP distribution on gliding sporozoites by immunofluorescence microscopy (Fig. 5D). WT sporozoites displayed the typical focal staining at the tips and deposition of TRAP in the trails. In marked contrast, in hsp20(-) sporozoites, TRAP was present in a single elongated region reminiscent of the attachment site seen in RICM (Fig. 5, C and D). Together, our data identify a key role for HSP20 in *in vitro* sporozoite motility likely by orchestrating the dynamics of parasite adhesion site formation and rupture.

Reduced Sporozoite Motility Does Not Affect Host Cell Traversal and Invasion—The current model for apicomplexan motility suggests that host cell entry and parasite locomotion are linked phenomena sharing the same molecular motor machinery (17, 57). In support of this model, several mutant sporozoites displaying defects in circular gliding motility were also invasion-deficient (56, 58 – 60). Therefore, our observation that hsp20(-) sporozoites exhibited normal *in vitro* and *in vivo* infectivity following intravenous injection despite their aberrant in vitro gliding motility is paradoxical. One possibility to reconcile these findings would be that motility parameters depend on the nature of the substrate used in the motility assay. Therefore, we wanted to compare gliding capacities of WT and hsp20(-) sporozoites on cultured fibroblasts and hepatoma cells. The former represent cellular barriers that need to be traversed by sporozoites en route to the liver, whereas the latter represent host cells, which are traversed and eventually invaded under simultaneous formation of a parasitophorous vacuole (61).

To permit live imaging, we first generated a new HSP20 knock-out parasite line, which expresses GFP under the control of the strong, sporozoite-specific promoter of the circumsporozoite protein (supplemental Fig. 4). Importantly, this parasite line, termed hsp20(-)::CS-GFP, independently confirmed the exclusive *in vivo* role for *HSP20* during mosquito-borne transmission as described above (supplemental Fig. 4, D and E). As a control, we used a parasite line that expresses the mCherry protein under the control of a constitutive Plasmodium HSP70 promoter that displays normal gliding and infectivity. We then performed live video microscopy using mixtures of WT::HSP70-mCherry and hsp20(-)::CS-GFP parasites on cultured cells (Fig. 6 and supplemental Movie 4). In parallel studies, individual parasite lines were recorded separately, giving rise to identical results.³ Notably, the reduction in the overall speed displayed by hsp20(-) sporozoites remained constant irrespective of the substrate (Fig. 6, A and B, and supplemental Fig. 5A), demonstrating that the speed defects are independent of the substrate and cannot be compensated by host cell surface ligands. When recorded over time, WT sporozoites displayed transient gliding periods interrupted by non-gliding phases (Fig. 6C). In contrast, hsp20(-) remained surface-attached at all times, indicating that the firm attachment observed on glass slides also occurs in contact with fibroblasts and hepatoma cells. This finding indicates an internal regulatory role of HSP20 in cellular motility because the phenotype of *HSP20* loss of function sporozoites is independent of the nature of the external ligands and topology of the substrate (supplemental Fig. 5, C and D).

The motility defects observed for hsp20(-) sporozoites in contact with cells may translate into reduced transmigration

³ G. N. Montagna, V. Brinkmann, and K. Matuschewski, unpublished data.



and invasion capacities. We tested this hypothesis by quantifying dextran-positive fibroblasts and hepatoma cells (Fig. 6D and supplemental Fig. 5B). WT and hsp20(-) sporozoites displayed no significant differences in their capacities to breach fibroblasts or hepatoma cells. We conclude that hsp20(-) sporozoites have a specific defect in fast and circular gliding motility but retain their full capacity to breach and eventually invade target

Fast Gliding Motility Is Essential for Migration in Host—So far, our findings indicate a direct link between fast motility and parasite movement during and/or after mosquito-borne inoculation of the vertebrate host. We hypothesized that the observed delay could be attributed to a defect of hsp20(-)sporozoites to move away from the probing site in the dermis to eventually enter a blood capillary. We therefore monitored sporozoite motility in vivo by intravital imaging (48). We observed that once injected into the skin of a host both WT and hsp20(-) sporozoites moved irregularly and showed seemingly random trajectories (Fig. 7A and supplemental Movies 5 and 6). As predicted, representative WT sporozoites (supplemental Movie 5) moved considerably faster inside the skin than hsp20(-) sporozoites (Fig. 7, B and C, and supplemental Movie 6). We next determined the meandering indices (Fig. 7*D*). This geometric parameter is the ratio of total displacement and path length of a cell track and a quantitative measure for the straightness of sporozoite movement. In vivo, WT and hsp20(-) sporozoites displayed a similar broad range of tracks as seen by the comparable meandering indices (Fig. 7D). Importantly, the difference in the overall speed between both parasite lines was similar to the difference observed previously in our in vitro assays. As a consequence, WT sporozoites showed a higher displacement capacity in the skin than hsp20(-) parasites (Fig. 7E). Because both populations apparently have the same pattern of movement *in vivo* (Fig. 7, A and D), the only discernible difference that accounts for the observed delay in patency is sporozoite speed.

We wanted to exclude that the observed delay could also be attributed to impaired release of hsp20(-) sporozoites from the mosquito proboscis. We observed that both WT and hsp20(-)sporozoites were typically seen at the tip of the proboscis and were able to move inside the proboscis. To discard the possibility that the delay could be due to a different amount of parasites at the bite site, we performed subcutaneous injections of equivalent amounts of WT and hsp20(-) sporozoites into naive mice (Fig. 7F). Reflecting our data from natural transmission (Fig. 4D), a large proportion (70%) of the animals remained malaria free, whereas some animals became malaria-positive after a delay of about 4 days. In conclusion, our data suggest that the delay in the infection observed in hsp20(-) parasites is caused exclusively by reduced motility in the dermis. This critical sporozoite function enables the parasite to efficiently move away from the inoculation site and enter the blood circulation.

DISCUSSION

In this study, using a molecular genetics approach in the single cell eukaryote Plasmodium, we established a direct role for a small heat shock protein in substrate-dependent cell motility.

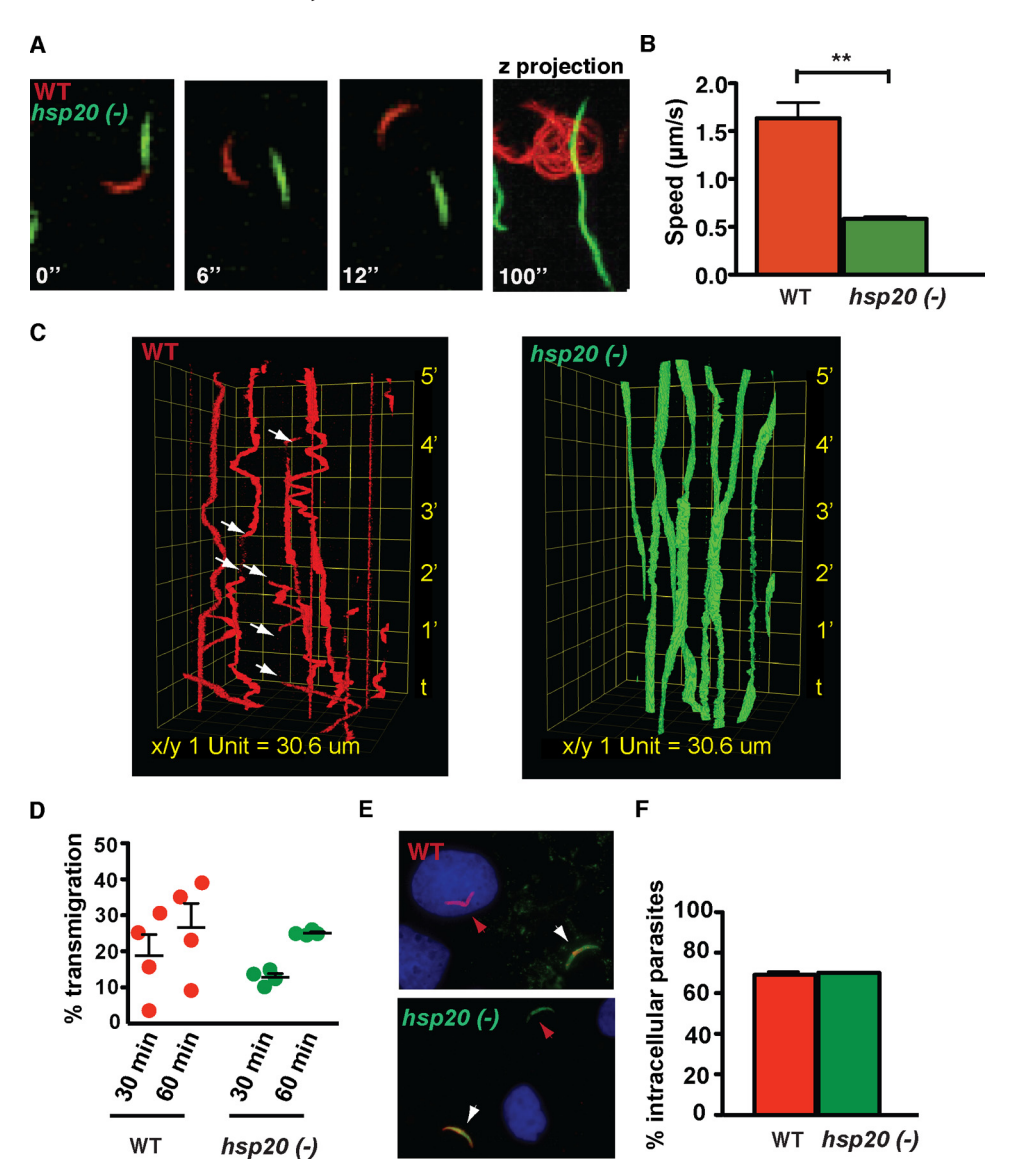


FIGURE 6. **Reduced gliding locomotion of** hsp20(-) **sporozoites on cultured cells.** A, time lapse images and temporal (z-) projection of mixed WT (red) and hsp20(-) sporozoites gliding on cultured fibroblasts. B, quantification of WT (red) and hsp20(-) (green) sporozoite speed in cultured fibroblasts. Shown are mean values of five experiments (\pm S.E.). Individual sporozoites were tracked between 1 and 8 min (WT, n=264; hsp20(-), n=497). **, p<0.05 (Mann-Whitney test). C, time lapse imaging of parasites presented as temporal projections (consecutive frames are stacked in the z-axis). WT sporozoites (red) alternate gliding periods with non-adherent or non-productive gliding phases, resulting in interrupted temporal projections. In contrast, hsp20(-) parasites (green) remain surface-attached during gliding on cultured fibroblasts, resulting in one continuous temporal projection. D, HSP20 ablation does not affect transmigration efficiency. Transmigration assays in cultured fibroblasts show comparable numbers of dextran-positive cells determined 30 and 60 min after inoculation of WT (red) or hsp20(-) (green) sporozoites. Shown are mean values of four experiments (\pm S.E.) ($n \ge 100$). E, invasion assays in hepatoma cells show that HSP20 deletion does not impair the ability of the sporozoite to invade target cells. Shown are indirect immunofluorescence micrographs of hepatoma cells incubated with WT (top) and hsp20(-) sporozoites (bottom). Red and white arrows indicate intra- and extracellular sporozoites, respectively. Extracellular parasites were stained with an anti-PbCS antibody (44). Note that in WT parasites expressing mCherry CS was detected using a green fluorescent secondary antibody. F, quantification of the proportion of intracellular WT and hsp20(-) parasites. Shown are mean values of four experiments (\pm S.E.) ($n \ge 100$). $Error bars \pm$ S.E.

Plasmodium sporozoites, the infectious transmission stage of the malaria parasite, display fast $(1-5~\mu\text{m/s})$, continuous, and circular substrate-dependent motility *in vitro*, termed gliding locomotion (54, 55, 57). *In vitro* sporozoite motility can be studied on artificial substrates, such as glass slides or flexible gels with high spatial and temporal resolution (34, 54, 55, 62). However, the *in vivo* relevance of the rapid sporozoite locomotion remained unclear. Multiple steps during the remarkably long sporozoite journey from the mosquito midgut to the hepatocyte may necessitate fast forward locomotion (63). Based on observational studies, gliding motility is thought to be critical

for at least six consecutive steps during host switch, including (i) sporozoite entry into the mosquito salivary glands, (ii) dispersion throughout the salivary duct system prior to a mosquito blood meal, (iii) intradermal migration from the mosquito bite site to neighboring blood or lymph vessels and their penetration, (iv) penetration of the endothelial barrier of the liver sinusoid, (v) migration through the liver parenchyma, and (vi) successful invasion of hepatocytes (48, 61, 64–66). Despite being abundantly expressed throughout the life cycle inside the mosquito vector and the observed impairment of ookinete speed, the important *in vivo* role of HSP20 is restricted to fast

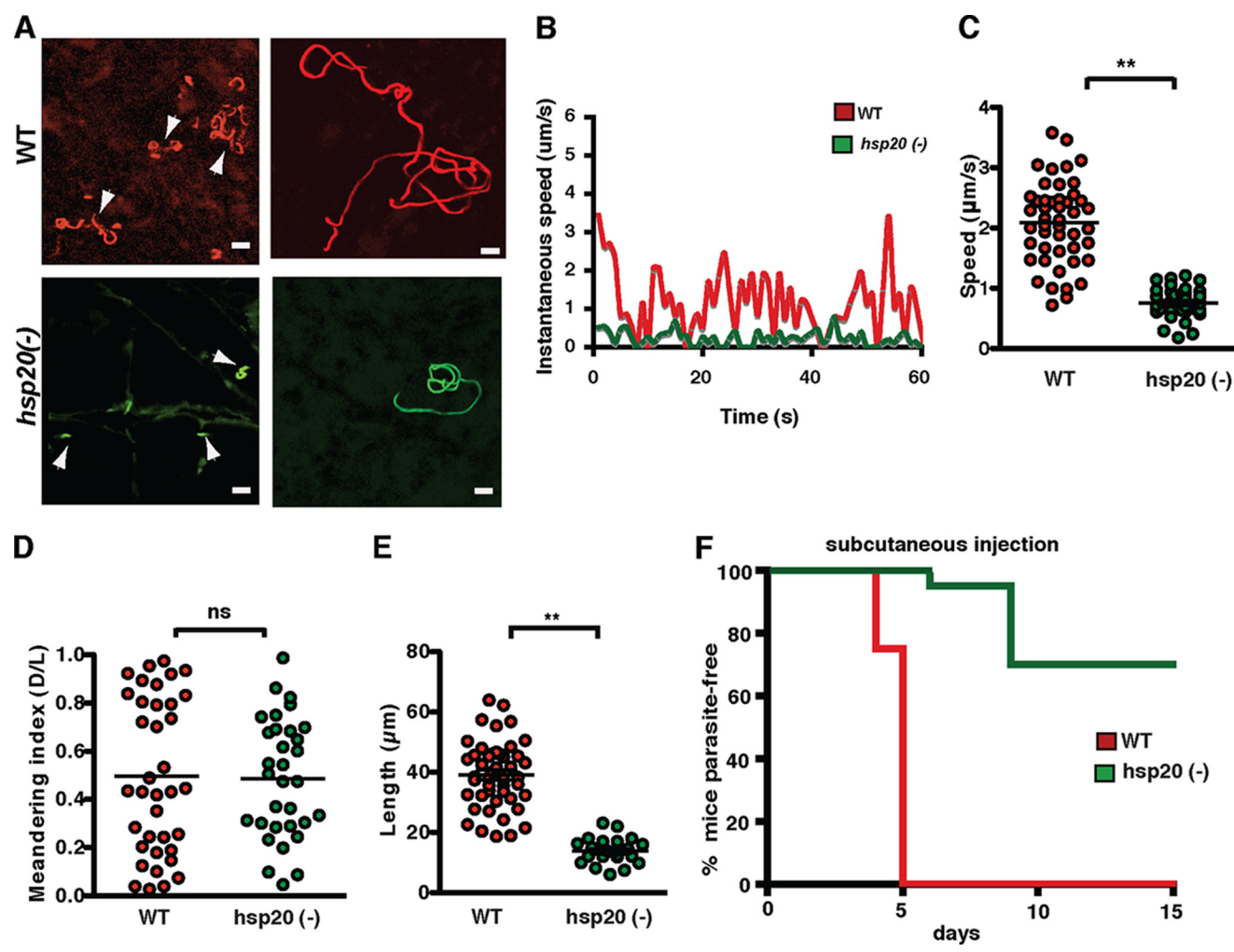


FIGURE 7. hsp20(-) sporozoites are severely impaired in intradermal migration. A, representative time lapse projections of WT (red) and hsp20(-) (green) sporozoites gliding within the mouse dermis. Graphs show the projections over a course of 5 min. Scale bars, 20 (left panels) and 10 µm (right panels). B, representative plot of instantaneous speed of WT (red) and hsp20(-) (green) sporozoites over a course of 1 min. C, sporozoites were quantified for speed within the dermis (WT, n = 47; hsp20(-), n = 35). D, quantification of the meandering index (total displacement/path length of a cell track (D/L)) (WT, n = 37; hsp20(-), n = 32). E, quantification of the total distance traveled in 30 s (WT, n = 45; hsp20(-), n = 25). C–E, shown are mean values (\pm S.D.). **, p < 0.05 (Mann-Whitney test); ns, non-significant. F, subcutaneous injection experiments. Mice were inoculated subcutaneously with 10,000 sporozoites (WT, n = 5; hsp20(-), n = 20).

sporozoite motility, which particularly affects parasite displacement in the skin.

Unexpectedly, hsp20(-) parasites did not display major defects in cellular transmigration or invasion of cultured fibroblast or hepatoma cells. These *in vitro* data are corroborated by our findings that bypassing the skin passage by intravenous injection of hsp20(-) sporozoites resulted in malaria infections that were indistinguishable from infections by wild type sporozoites. This finding appears to contradict the notion that Apicomplexa use the identical motor machinery for locomotion, cell penetration, and invasion. It was proposed that these processes involve different ligands, which may engage distinct signaling pathways and regulatory proteins that integrate a shared molecular motor (57). Our findings provide a proof for this concept. Although many motor proteins and surface proteins, such as TRAP invasins, are shared for all functions, regulators, such as HSP20, apparently exert their crucial role during a brief moment in the life cycle when parasites need to perform fast gliding motility.

We show here that HSP20 polarization and translocation to the cortical space are signatures of mature Plasmodium sporozoites, which perform overall continuous substrate-dependent locomotion. Intriguingly, the proportion of sporozoites displaying apical and bipolar HSP20 localization correlates with the fraction of motile parasites. Because this pattern of localization is unprecedented for a protein involved in gliding motility, an interesting question is how is HSP20 recruited to the sporozoite periphery. Most apicomplexan HSP20 proteins contain a conserved cysteine residue at position 3 that could potentially be palmitoylated and hence may mediate reversible insertion into lipid bilayers. Recombinant TgHSP20 interacts with classical phospholipids, e.g. phosphatidylinositol 4-phospate or phosphatidylinositol 4,5-bisphospate (42). This class of signaling molecules regulates among others actin nucleators and cytoskeletal and membrane-associated proteins (67). A class of actin regulators, termed Enabled/vasodilator-stimulated phosphoprotein (ENA/VASP) proteins, can act as both positive and negative regulators of cell speed in diverse cell types (68). These



proteins control the actin filament network and thereby regulate fibroblast motility, neutrophil migration, and chemotaxis efficiency in *Dictyostelium discoideum* (69). Accumulation of VASP at the leading edge of fish keratocytes correlates with speed and movement coherency (70). HSP20 localization to the parasite tips during gliding supports the hypothesis that HSP20 could regulate the activity of actin-binding proteins.

Recently, quantitative microscopy-based assays revealed that sporozoite motility is limited by the dynamic turnover of discrete adhesion sites (34). It is tempting to speculate that the polarized pattern of HSP20 localization reflects the discrete adhesion zones, which retain their spatial localization during cellular motility. In support of this notion, our RICM studies revealed an aberrant uniform adhesion zone and slow linear motion in sporozoites that lack HSP20. The elongated adhesion sites in hsp20(-) sporozoites allowed us to directly test the hypothesis that RICM visualizes TRAP-positive adhesion sites. Indeed, TRAP displayed a uniform, elongated distribution in hsp20(-) sporozoites that was very distinct from the focal pattern in WT sporozoites. Together, our findings suggest that HSP20 regulates the turnover of attachment sites.

One alternative possibility is that HSP20 directly contributes to cell-substrate adhesion, *i.e.* by physical interaction with transmembrane parasite invasins. A prediction would be that more attachment interactions occur during the three-dimensional movement in the dermis, suggesting that the *hsp20(-)* phenotype should be more pronounced *in vivo*. However, *hsp20(-)* sporozoites displayed a roughly uniform overall speed reduction irrespective of their substrate, *i.e.* glass slide, cultured cells, or within the skin. The most plausible explanation is that HSP20 modulates the motor complex that generates the traction forces during sporozoite locomotion. HSP20 could regulate the turnover of actin polymerization, compete with actomyosin interaction, or both. The chaperone activity may also contribute to the integrity of the motor complex interactions (for instance binding of aldolase tetramers to TRAP).

It is important to stress that HSP20 is not essential for parasite life cycle progression. It plays a critical role when the pathogen is transmitted naturally, and a substantial number of animals remained malaria-free after infection by mosquito bite. Those animals that became infected displayed a consistent delay in the time to parasite detection in the peripheral blood. Therefore, the loss of HSP20 function is distinct from the abolishment of malaria transmission described for Plasmodium invasins and surface molecules (56, 58, 59) and microfilament regulators, such as capping protein (60). These mutant parasites failed to colonize salivary glands of the mosquito vector, precluding a direct analysis of additional roles during sporozoite transmission. On the other hand, Plasmodium proteins with critical roles in cell traversal activity all displayed normal sporozoite gliding locomotion (71, 72). Only the intermediate phenotype observed for hsp20(-) sporozoites permitted the assessment of the *in vivo* role of fast parasite motility.

A delay in parasite detection can be explained by greatly reduced numbers of sporozoites that eventually breach a capillary and enter the bloodstream. Moreover, hsp20(-) sporozoites displayed normal traversal activity, supporting the concept that reduced gliding locomotion is the direct cause of the

impaired mosquito-to-mouse transmission. We speculate that variations in malaria infections, ranging from delayed to no infection at all, reflect the relative distance of blood vessels from the inoculation site.

We performed the infections with a small number of infected mosquitoes, most likely reflecting malaria transmission in endemic areas. In fact, typically only up to 5% of all female anopheline mosquitoes are infectious even in areas of holoendemicity (73). In this context, the observed defect in malaria transmission may be of significance for the design of malaria intervention strategies. Work in rodent models showed that protective antisporozoite immune responses are primarily induced by sporozoites that are flushed away from the inoculation site to the draining lymph nodes (74). Specific inhibition of *HSP20*-mediated fast sporozoite motility may therefore not only significantly reduce the sporozoite inoculum and hence benefit disease outcome, but it may also augment protective immunity against live whole-cell *Plasmodium* parasites.

Acknowledgments—We acknowledge Dr. Sergio Angel (Instituto de Investigaciones Biotecnológicas (IIB-INTECH)) for continuous critical discussions. We thank Diana Scheppan for expert technical assistance.

REFERENCES

- Pollard, T. D., and Borisy, G. G. (2003) Cellular motility driven by assembly and disassembly of actin filaments. Cell 112, 453–465
- Pollard, T. D., and Cooper, J. A. (2009) Actin, a central player in cell shape and movement. Science 326, 1208 –1212
- 3. Miron, T., Wilchek, M., and Geiger, B. (1988) Characterization of an inhibitor of actin polymerization in vinculin-rich fraction of turkey gizzard smooth muscle. *Eur. J. Biochem.* **178**, 543–553
- 4. Miron, T., Vancompernolle, K., Vandekerckhove, J., Wilchek, M., and Geiger, B. (1991) A 25-kD inhibitor of actin polymerization is a low molecular mass heat shock protein. *J. Cell Biol.* **114**, 255–261
- 5. Lindquist, S., and Craig, E. A. (1988) The heat-shock proteins. *Annu. Rev. Genet.* **22**, 631–677
- Narberhaus, F. (2002) α-Crystallin-type heat shock proteins: socializing minichaperones in the context of a multichaperone network. *Microbiol. Mol. Biol. Rev.* 66, 64 – 93
- Kim, K. K., Kim, R., and Kim, S. H. (1998) Crystal structure of a small heat-shock protein. *Nature* 394, 595–599
- 8. Haslbeck, M., Franzmann, T., Weinfurtner, D., and Buchner, J. (2005) Some like it hot: the structure and function of small heat-shock proteins. *Nat. Struct. Mol. Biol.* **12**, 842–846
- 9. Lavoie, J. N., Gingras-Breton, G., Tanguay, R. M., and Landry, J. (1993) Induction of Chinese hamster HSP27 gene expression in mouse cells confers resistance to heat shock. HSP27 stabilization of the microfilament organization. *J. Biol. Chem.* **268**, 3420–3429
- Benndorf, R., Hayess, K., Ryazantsev, S., Wieske, M., Behlke, J., and Lutsch, G. (1994) Phosphorylation and supramolecular organization of murine small heat shock protein HSP25 abolish its actin polymerization-inhibiting activity. J. Biol. Chem. 269, 20780 – 20784
- Lavoie, J. N., Lambert, H., Hickey, E., Weber, L. A., and Landry, J. (1995) Modulation of cellular thermoresistance and actin filament stability accompanies phosphorylation-induced changes in the oligomeric structure of heat shock protein 27. Mol. Cell. Biol. 15, 505–516
- Gu, J., Emerman, M., and Sandmeyer, S. (1997) Small heat shock protein suppression of Vpr-induced cytoskeletal defects in budding yeast. *Mol. Cell. Biol.* 17, 4033–4042
- Rembold, C. M., Foster, D. B., Strauss, J. D., Wingard, C. J., and Eyk, J. E. (2000) cGMP-mediated phosphorylation of heat shock protein 20 may cause smooth muscle relaxation without myosin light chain dephospho-



- rylation in swine carotid artery. J. Physiol. 524, 865-878
- 14. Edwards, H. V., Cameron, R. T., and Baillie, G. S. (2011) The emerging role of HSP20 as a multifunctional protective agent. Cell. Signal. 23, 1447-1454
- 15. Dreiza, C. M., Brophy, C. M., Komalavilas, P., Furnish, E. J., Joshi, L., Pallero, M. A., Murphy-Ullrich, J. E., von Rechenberg, M., Ho, Y. S., Richardson, B., Xu, N., Zhen, Y., Peltier, J. M., and Panitch, A. (2005) Transducible heat shock protein 20 (HSP20) phosphopeptide alters cytoskeletal dynamics. FASEB J. 19, 261–263
- 16. Karolczak-Bayatti, M., Sweeney, M., Cheng, J., Edey, L., Robson, S. C., Ulrich, S. M., Treumann, A., Taggart, M. J., and Europe-Finner, G. N. (2011) Acetylation of heat shock protein 20 (Hsp20) regulates human myometrial activity. J. Biol. Chem. 286, 34346-34355
- 17. Sibley, L. D. (2004) Intracellular parasite invasion strategies. Science 304,
- 18. Sattler, J. M., Ganter, M., Hliscs, M., Matuschewski, K., and Schüler, H. (2011) Actin regulation in the malaria parasite. Eur. J. Cell Biol. 90,
- 19. Meissner, M., Schlüter, D., and Soldati, D. (2002) Role of Toxoplasma gondii myosin A in powering parasite gliding and host cell invasion. Science **298**, 837 – 840
- 20. Bergman, L. W., Kaiser, K., Fujioka, H., Coppens, I., Daly, T. M., Fox, S., Matuschewski, K., Nussenzweig, V., and Kappe, S. H. (2003) Myosin A tail domain interacting protein (MTIP) localizes to the inner membrane complex of *Plasmodium* sporozoites. *J. Cell Sci.* 116, 39 – 49
- 21. Heaslip, A. T., Leung, J. M., Carey, K. L., Catti, F., Warshaw, D. M., Westwood, N. J., Ballif, B. A., and Ward, G. E. (2010) A small-molecule inhibitor of *T. gondii* motility induces the posttranslational modification of myosin light chain-1 and inhibits myosin motor activity. PLoS Pathog. 6, e1000720
- 22. Siden-Kiamos, I., Ganter, M., Kunze, A., Hliscs, M., Steinbüchel, M., Mendoza, J., Sinden, R. E., Louis, C., and Matuschewski, K. (2011) Stage-specific depletion of myosin A supports an essential role in motility of malarial ookinetes. Cell. Microbiol. 13, 1996-2006
- 23. Schüler, H., Mueller, A. K., and Matuschewski, K. (2005) Unusual properties of Plasmodium falciparum actin: new insights into microfilament dynamics of apicomplexan parasites. FEBS Lett. 579, 655-660
- 24. Schmitz, S., Grainger, M., Howell, S., Calder, L. J., Gaeb, M., Pinder, J. C., and Holder, A. A., and Veigel, C. (2005) Malaria parasite actin filaments are very short. J. Mol. Biol. 349, 113-125
- 25. Schmitz, S., Schaap, I. A., Kleinjung, J., Harder, S., Grainger, M., Calder, L., Rosenthal, P. B., Holder, A. A., and Veigel, C. (2010) Malaria parasite actin polymerization and filament structure. J. Biol. Chem. 285, 36577-36585
- 26. Sahoo, N., Beatty, W., Heuser, J., Sept, D., and Sibley, L. D. (2006) Unusual kinetic and structural properties control rapid assembly and turnover of actin in the parasite Toxoplasma gondii. Mol. Biol. Cell 17, 895-906
- 27. Heiss, K., Nie, H., Kumar, S., Daly, T. M., Bergman, L. W., and Matuschewski, K. (2008) Functional characterization of a redundant Plasmodium TRAP family invasin, TRAP-like protein, by aldolase binding and a genetic complementation test. Eukaryot. Cell 7, 1062-1070
- 28. Lacroix, C., and Ménard, R. (2008) TRAP-like protein of Plasmodium sporozoites: linking gliding motility to host-cell traversal. Trends Parasitol. 24, 431-434
- 29. Jewett, T. J., and Sibley, L. D. (2003) Aldolase forms a bridge between cell surface adhesins and the actin cytoskeleton in apicomplexan parasites. Mol. Cell 11, 885-894
- 30. Buscaglia, C. A., Coppens, I., Hol, W. G., and Nussenzweig, V. (2003) Sites of interaction between aldolase and thrombospondin-related anonymous protein in Plasmodium. Mol. Biol. Cell 14, 4947-4957
- 31. Bosch, J., Buscaglia, C. A., Krumm, B., Ingason, B. P., Lucas, R., Roach, C., Cardozo, T., Nussenzweig, V., and Hol, W. G. (2007) Aldolase provides an unusual binding site for thrombospondin-related anonymous protein in the invasion machinery of the malaria parasite. Proc. Natl. Acad. Sci. U.S.A. 104, 7015-7020
- 32. Shaw, M. K., and Tilney, L. G. (1999) Induction of an acrosomal process in Toxoplasma gondii: visualization of actin filaments in a protozoan parasite. Proc. Natl. Acad. Sci. U.S.A. 96, 9095-9099
- 33. Wetzel, D. M., Håkansson, S., Hu, K., Roos, D., and Sibley, L. D. (2003) Actin filament polymerization regulates gliding motility by apicomplexan

- parasites. Mol. Biol. Cell 14, 396 406
- 34. Münter, S., Sabass, B., Selhuber-Unkel, C., Kudryashev, M., Hegge, S., Engel, U., Spatz, J. P., Matuschewski, K., Schwarz, U. S., and Frischknecht, F. (2009) Plasmodium sporozoite motility is modulated by the turnover of discrete adhesion sites. Cell Host Microbe 6, 551–562
- 35. Plattner, F., Yarovinsky, F., Romero, S., Didry, D., Carlier, M. F., Sher, A., and Soldati-Favre, D. (2008) Toxoplasma profilin is essential for host cell invasion and TLR11-dependent induction of an interleukin-12 response. *Cell Host Microbe* **3,** 77–87
- 36. Kursula, I., Kursula, P., Ganter, M., Panjikar, S., Matuschewski, K., and Schüler, H. (2008) Structural basis for parasite-specific functions of the divergent profilin of *Plasmodium falciparum*. Structure 16, 1638-1648
- 37. Schüler, H., Mueller, A. K., and Matuschewski, K. (2005) A Plasmodium actin-depolymerizing factor that binds exclusively to actin monomers. Mol. Biol. Cell 16, 4013-4023
- 38. Mehta, S., and Sibley, L. D. (2010) Toxoplasma gondii actin depolymerizing factor acts primarily to sequester G-actin. J. Biol. Chem. 285, 6835 - 6847
- 39. Hliscs, M., Sattler, J. M., Tempel, W., Artz, J. D., Dong, A., Hui, R., Matuschewski, K., and Schüler, H. (2010) Structure and function of a G-actin sequestering protein with a vital role in malaria oocyst development inside the mosquito vector. J. Biol. Chem. 285, 11572–11583
- Baum, J., Papenfuss, A. T., Baum, B., Speed, T. P., and Cowman, A. F. (2006) Regulation of apicomplexan actin-based motility. Nat. Rev. Microbiol. 4, 621-628
- 41. Schüler, H., and Matuschewski, K. (2006) Regulation of apicomplexan microfilament dynamics by a minimal set of actin-binding proteins. Traffic 7, 1433-1439
- 42. de Miguel, N., Lebrun, M., Heaslip, A., Hu, K., Beckers, C. J., Matrajt, M., Dubremetz, J. F., and Angel, S. O. (2008) Toxoplasma gondii Hsp20 is a stripe-arranged chaperone-like protein associated with the outer leaflet of the inner membrane complex. Biol. Cell 100, 479 - 489
- 43. Janse, C. J., Franke-Fayard, B., Mair, G. R., Ramesar, J., Thiel, C., Engelmann, S., Matuschewski, K., van Gemert, G. J., Sauerwein, R. W., and Waters, A. P. (2006) High efficiency transfection of Plasmodium berghei facilitates novel selection procedures. Mol. Biochem. Parasitol. 145, 60 - 70
- 44. Potocnjak, P., Yoshida, N., Nussenzweig, R. S., and Nussenzweig, V. (1980) Monovalent fragments (Fab) of monoclonal antibodies to a sporozoite surface antigen (Pb44) protect mice against malarial infection. J. Exp. Med. **151,** 1504 – 1513
- 45. Tsuji, M., Mattei, D., Nussenzweig, R. S., Eichinger, D., and Zavala, F. (1994) Demonstration of heat-shock protein 70 in the sporozoite stage of malaria parasites. Parasitol. Res. 80, 16-21
- 46. Goosmann, C., Abed, U. A., and Brinkmann, V. (2008) Infection at the cellular level. Methods Cell Biol. 88, 477-496
- 47. Moon, R. W., Taylor, C. J., Bex, C., Schepers, R., Goulding, D., Janse, C. J., Waters, A. P., Baker, D. A., and Billker, O. (2009) A cyclic GMP signalling module that regulates gliding motility in a malaria parasite. PLoS Pathog.
- 48. Amino, R., Thiberge, S., Martin, B., Celli, S., Shorte, S., Frischknecht, F., and Ménard R (2006) Quantitative imaging of *Plasmodium* transmission from mosquito to mammal. Nat. Med. 12, 220-224
- Aurrecoechea, C., Brestelli, J., Brunk, B. P., Dommer, J., Fischer, S., Gajria, B., Gao, X., Gingle, A., Grant, G., Harb, O. S., Heiges, M., Innamorato, F., Iodice, J., Kissinger, J. C., Kraemer, E., Li, W., Miller, J. A., Nayak, V., Pennington, C., Pinney, D. F., Roos, D. S., Ross, C., Stoeckert, C. J., Jr., Treatman, C., and Wang, H.(2009) PlasmoDB: a functional genomic database for malaria parasites. Nucleic Acids Res. 37, D539-D543
- 50. van Montfort, R. L., Basha, E., Friedrich, K. L., Slingsby, C., and Vierling, E. (2001) Crystal structure and assembly of a eukaryotic small heat shock protein. Nat. Struct. Biol. 8, 1025-1030
- Shaner, N. C., Campbell, R. E., Steinbach, P. A., Giepmans, B. N., Palmer, A. E., and Tsien, R. Y. (2004) Improved monomeric red, orange and yellow fluorescent proteins derived from *Discosoma* sp. red fluorescent protein. Nat. Biotechnol. 22, 1567–1572
- 52. Meis, J. F., Verhave, J. P., Jap, P. H., and Meuwissen, J. H. (1985) Transformation of sporozoites of Plasmodium berghei into exoerythrocytic forms



- in the liver of its mammalian host. Cell Tissue Res. 241, 353-360
- Jayabalasingham, B., Bano, N., and Coppens, I. (2010) Metamorphosis of the malaria parasite in the liver is associated with organelle clearance. *Cell Res.* 20, 1043–1059
- 54. Vanderberg, J. P. (1974) Studies on the motility of *Plasmodium* sporozoites. *J. Protozool.* **21**, 527–537
- Vanderberg, J. P. (1975) Development of infectivity by the *Plasmodium berghei* sporozoite. *J. Parasitol.* 61, 43–50
- Sultan, A. A., Thathy, V., Frevert, U., Robson, K. J., Crisanti, A., Nussenzweig, V., Nussenzweig, R. S., and Ménard, R. (1997) TRAP is necessary for gliding motility and infectivity of *Plasmodium* sporozoites. *Cell* 90, 511–522
- 57. Ménard, R. (2001) Gliding motility and cell invasion by Apicomplexa: insights from the *Plasmodium* sporozoite. *Cell. Microbiol.* **3,** 63–73
- 58. Steinbuechel, M., and Matuschewski, K. (2009) Role for the *Plasmodium* sporozoite-specific transmembrane protein S6 in parasite motility and efficient malaria transmission. *Cell. Microbiol.* **11**, 279 288
- Engelmann, S., Silvie, O., and Matuschewski, K. (2009) Disruption of *Plas-modium* sporozoite transmission by depletion of sporozoite invasion-associated protein 1. *Eukaryot. Cell* 8, 640 648
- Ganter, M., Schüler, H., and Matuschewski, K. (2009) Vital role for the Plasmodium actin capping protein (CP) β-subunit in motility of malaria sporozoites. Mol. Microbiol. 74, 1356–1367
- Mota, M. M., Pradel, G., Vanderberg, J. P., Hafalla, J. C., Frevert, U., Nussenzweig, R. S., Nussenzweig, V., and Rodríguez, A. (2001) Migration of *Plasmodium* sporozoites through cells before infection. *Science* 291, 141–144
- Hegge, S., Münter, S., Steinbüchel, M., Heiss, K., Engel, U., Matuschewski, K., and Frischknecht, F. (2010) Multistep adhesion of *Plasmodium* sporozoites. *FASEB J.* 24, 2222–2234
- Kappe, S. H., Kaiser, K., and Matuschewski, K. (2003) The *Plasmodium* sporozoite journey: a rite of passage. *Trends Parasitol.* 19, 135–143
- 64. Frischknecht, F., Baldacci, P., Martin, B., Zimmer, C., Thiberge, S., Olivo-Marin, J. C., Shorte, S. L., and Ménard, R. (2004) Imaging movement of

- malaria parasites during transmission by *Anopheles* mosquitoes. *Cell. Microbiol.* **6.** 687–694
- Matuschewski, K. (2006) Getting infectious: formation and maturation of *Plasmodium* sporozoites in the *Anopheles* vector. *Cell. Microbiol.* 8, 1547–1556
- Frevert, U., Engelmann, S., Zougbédé, S., Stange, J., Ng, B., Matuschewski, K., Liebes, L., and Yee, H. (2005) Intravital observation of *Plasmodium berghei* sporozoite infection of the liver. *PLoS Biol.* 3, e192
- 67. Campellone, K. G., and Welch, M. D. (2010) A nucleator arms race: cellular control of actin assembly. *Nat. Rev. Mol. Cell Biol.* 11, 237–251
- Bear, J. E., Loureiro, J. J., Libova, I., Fässler, R., Wehland, J., and Gertler,
 F. B. (2000) Negative regulation of fibroblast motility by Ena/VASP proteins. *Cell* 101, 717–728
- Krause, M., Dent, E. W., Bear, J. E., Loureiro, J. J., and Gertler, F. B. (2003)
 Ena/VASP proteins: regulators of the actin cytoskeleton and cell migration. *Annu. Rev. Cell Dev. Biol.* 19, 541–564
- Lacayo, C. I., Pincus, Z., VanDuijn, M. M., Wilson, C. A., Fletcher, D. A., Gertler, F. B., Mogilner, A., and Theriot, J. A. (2007) Emergence of large-scale cell morphology and movement from local actin filament growth dynamics. *PLoS Biol.* 5, e233
- Ishino, T., Yano, K., Chinzei, Y., and Yuda, M. (2004) Cell-passage activity is required for the malarial parasite to cross the liver sinusoidal cell layer. *PLoS Biol.* 2, E4
- 72. Bhanot, P., Schauer, K., Coppens, I., and Nussenzweig, V. (2005) A surface phospholipase is involved in the migration of *Plasmodium* sporozoites through cells. *J. Biol. Chem.* **280**, 6752–6760
- Kleinschmidt, I., Schwabe, C., Benavente, L., Torrez, M., Ridl, F. C., Segura, J. L., Ehmer, P., and Nchama, G. N. (2009) Marked increase in child survival after four years of intensive malaria control. *Am. J. Trop. Med. Hyg.* 80, 882–888
- Chakravarty, S., Cockburn, I. A., Kuk, S., Overstreet, M. G., Sacci, J. B., and Zavala, F. (2007) CD8⁺ T lymphocytes protective against malaria liver stages are primed in skin-draining lymph nodes. *Nat. Med.* 13, 1035–1041

